Materials Today Bio 28 (2024) 101197

Contents lists available at ScienceDirect

Materials Today Bio

journal homepage: www.journals.elsevier.com/materials-today-bio

Dual roles of photosynthetic hydrogel with sustained oxygen generation in promoting cell survival and eradicating anaerobic infection

Jun Kang [a], Ye Liang [a], Junqing Liu [a], Mingxin Hu [a], Shulan Lin [a], Jialin Zhong [a], Chaogang Wang [b], Qinglu Zeng [c], Chengfei Zhang [a,*]

[a] Restorative Dental Sciences, Faculty of Dentistry, The University of Hong Kong, Hong Kong, China
[b] Guangdong Technology Research Center for Marine Algal Bioengineering, College of Life Sciences and Oceanography, Shenzhen University, Shenzhen 518060, China
[c] Department of Ocean Science, The Hong Kong University of Science and Technology, Hong Kong, China

ARTICLE INFO

Keywords:
Antibacterial activity
Anaerobic bacteria
Chlamydomonas reinhardtii
Oxygen
Photosynthesis
Tissue engineering

ABSTRACT

Tissue engineering offers a promising alternative for oral and maxillofacial tissue defect rehabilitation; however, cells within a sizeable engineered tissue construct after transplantation inevitably face prolonged and severe hypoxic conditions, which may compromise the survivability of the transplanted cells and arouse the concern of anaerobic infection. Microalgae, which can convert carbon dioxide and water into oxygen and glucose through photosynthesis, have been studied as a source of oxygen supply for several biomedical applications, but their promise in orofacial tissue regeneration remains unexplored. Here, we demonstrated that through photosynthetic oxygenation, *Chlamydomonas reinhardtii* (*C. reinhardtii*) supported dental pulp stem cell (DPSC) energy production and survival under hypoxia. We developed a multifunctional photosynthetic hydrogel by embedding DPSCs and *C. reinhardtii* encapsulated alginate microspheres (CAMs) within gelatin methacryloyl hydrogel (GelMA) (CAMs@GelMA). This CAMs@GelMA hydrogel can generate a sustainable and sufficient oxygen supply, reverse intracellular hypoxic status, and enhance the metabolic activity and viability of DPSCs. Furthermore, the CAMs@GelMA hydrogel exhibited selective antibacterial activity against oral anaerobes and remarkable antibiofilm effects on multispecies biofilms by disrupting the hypoxic microenvironment and increasing reactive oxygen species generation. Our work presents an innovative photosynthetic strategy for oral tissue engineering and opens new avenues for addressing other hypoxia-related challenges.

1. Introduction

In recent decades, tissue engineering has emerged as a promising strategy for the regeneration of damaged/lost oral and maxillofacial tissues, including dentin-pulp complex [1,2], periodontal tissue [3], bone [4], cartilage [5], and salivary gland [6]. Nevertheless, clinical translation of these engineered tissue constructs is greatly hindered by the low survivability of transplanted cells, primarily attributed to insufficient oxygen and nutrient supply [7]. Oxygen, usually transported through the circulation system, is indispensable for cell metabolism, energy supply, and survival [8]. Thus, tissue vascularization to establish functional blood circulation is essential for long-lasting oxygen delivery [9]. Due to the slow ingrowth of host vasculature, the transplanted tissues, if located beyond limited passive oxygen diffusion, would suffer ischemia and hypoxia during the early post-implantation stage, leading to cell/tissue necrosis, even transplant failure [10–12]. Hence, novel strategies that enable immediate and sustained oxygen supply before vascularization occurs present a key stepping stone in maintaining cell/tissue survival and metabolism.

To mitigate tissue hypoxia independently of blood vessel perfusion, a variety of oxygen-supplying systems have been explored, including hyperbaric oxygen therapy [13], oxygen-delivering carriers (e.g., fluorinated compounds and hemoglobin) [14,15], and oxygen-generating materials (e.g., peroxides and sodium percarbonates with catalase) [16–18]. These strategies offer seeded cells a more hospitable environment upon implantation, supporting their survival and function; yet, various limitations remain, including pulmonary barotrauma, low oxygen-carrying capacity, burst oxygen release, short duration of oxygen generation, cytotoxic byproducts such as hydrogen peroxide (H_2O_2) and reactive oxygen species (ROS), and accumulation of metabolic waste like carbon dioxide (CO_2) [19,20]. Thus, new insights into developing a biocompatible material that can provide controllable

* Corresponding author.
E-mail address: zhangcf@hku.hk (C. Zhang).

https://doi.org/10.1016/j.mtbio.2024.101197
Received 2 June 2024; Received in revised form 27 July 2024; Accepted 8 August 2024
Available online 10 August 2024

oxygen supply and waste removal are of utmost clinical significance.

Drawing inspiration from symbiotic recycling systems, where photosynthetic organisms use metabolites and wastes from their hosts to generate oxygen and organic carbon metabolites for animals [21], the incorporation of photosynthetic microorganisms into hypoxic tissues as a source of oxygen supply has unlocked new perspectives in the treatment of hypoxia-related diseases [22,23]. *Chlamydomonas reinhardtii* (*C. reinhardtii*), a spherical unicellular green microalga, exhibits photosynthetic capability, enabling carbon dioxide consumption and oxygen production upon light exposure [24]. Due to its superior photosynthetic efficiency, ease of cultivation, rapid growth rates, amenability to genetic manipulation, and excellent biocompatibility, *C. reinhardtii* has been proposed as a potent oxygen generator for various biomedical applications, including wound healing [25,26], tissue engineering [27,28], rescuing avascularized brain tissue [29], cancer treatment [30], and organ transplantation [31]. Several *in vivo* studies and clinical trials have already demonstrated the feasibility and biosafety of this photosynthetic therapy [25,26,32]. Unlike previous studies that focused solely on immobilizing microalgae within biomaterials, the present research makes a distinctive contribution by co-encapsulating stem cells and microalgae within engineered tissue constructs, thereby utilizing photosynthetically-generated oxygen from microalgae to support stem cell survival.

In addition, many microorganisms harbor in the oral and maxillofacial environments, including aerobic and anaerobic commensal and pathogenic species [33,34]. Critically, some hypoxic regions, such as root canals and deep periodontal pockets, favor anaerobic pathogen colonizing and proliferation [35,36], which can lead to anaerobe-related infections, triggering host immune cell attacks and the release of inflammatory factors, which, in turn, impairs the new tissue formation [37]. Conversely, local oxygen enrichment can positively influence the dysbiotic oral microflora, inhibiting the proliferation of anaerobic bacteria [38,39]. Therefore, incorporating microalgae into engineered tissue constructs may maintain aerobic conditions by providing sufficient oxygen and eventually prevent or eliminate anaerobic infections. To the best of our knowledge, this study represents the first attempt to employ microalgae as a source of photosynthetic oxygen for controlling anaerobic infection.

Herein, we developed a multifunctional photosynthetic hydrogel in which *C. reinhardtii* was initially immobilized into alginate microspheres and then co-encapsulated with dental pulp stem cells (DPSCs) within a photo-cross-linkable gelatin methacryloyl (GelMA) hydrogel (Scheme 1). We hypothesized that *C. reinhardtii* would alleviate the hypoxic environment via photosynthesis-derived oxygen, promoting DPSC survival and destroying the anaerobic infection. The hydrogel's microstructure, oxygen release kinetics, and DPSC metabolic activity, viability, and energy production were evaluated. In addition, the hydrogel's antimicrobial and antibiofilm properties were explored. The present study serves as a proof of concept for utilizing photosynthetic biomaterials to address hypoxia-associated issues in transplanted engineered tissues.

2. Materials and methods

2.1. Cell culture

One *C. reinhardtii* strain JUV, obtained from Guangdong Technology Research Center for Marine Algal Bioengineering, Shenzhen University, was grown photomixotrophically in liquid Tris-Acetate-Phosphate medium (TAP; Thermo Fisher Scientific, Carlsbad, CA, USA) or on solid TAP agar plates with 100 μg/mL ampicillin (Mei5 Biotechnology, Beijing, China) at 25 °C in an illuminated incubator, utilizing the full spectrum of white light (4500 lux) [40]. DPSCs were purchased from Lonza (Basel, Switzerland) and cultured in α-modified Eagle's medium (αMEM; Thermo Fisher Scientific) supplemented with 10 % (v/v) fetal bovine serum (FBS; Thermo Fisher Scientific) and 1 % (v/v) penicillin/streptomycin (Sigma-Aldrich, St. Louis, MO, USA) at 37 °C and 5 % CO_2 in a humidified incubator.

For cell coculture in two-dimension (2D), DPSCs were seeded onto 24-well plates at a density of 5×10^4 cells per well and incubated overnight at 37 °C. Next, 0.4 μm pore transwell inserts (Jet Bio-Filtration, Guangzhou, China) loaded with varying concentrations of *C. reinhardtii* (0, 5, 10, and 20×10^6 microalgae/mL) were gently placed into the 24-well plates, followed by indirect coculture in a normoxic (21 % O_2, 5 % CO_2) or hypoxic (1 % O_2, 5 % CO_2) incubator at 35 °C with continuous exposure to white light (4500 lux) (Fig. 2a). A 1:1 mixture of αMEM-10 % FBS and TAP medium was used as the coculture medium.

2.2. Immobilization of C. reinhardtii in alginate microspheres

5 % (w/v) alginic acid sodium salt from brown algae (low viscosity, Sigma-Aldrich) was dissolved into TAP medium under continuous

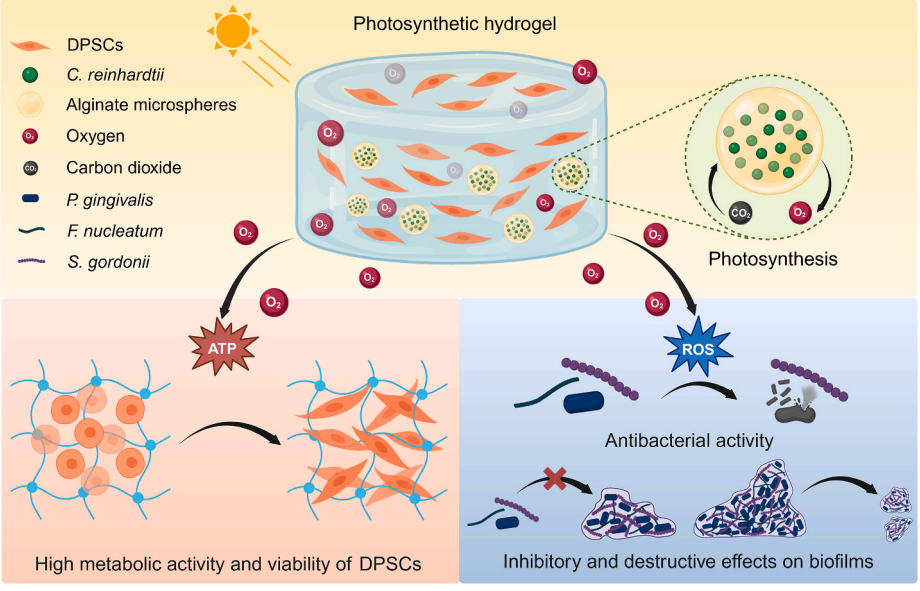

Scheme 1. The photosynthetic hydrogel could provide sustained and sufficient oxygen supply through photosynthesis by encapsulating *C. reinhardtii* alginate microspheres to promote DPSC survival and eradicate anaerobic infection.

stirring at 37 °C for 5 h and then sterilized with a 0.22 μm filter [41]. 2.5 % (w/v) calcium chloride ($CaCl_2$; Sigma-Aldrich) solution was prepared by dissolving $CaCl_2$ powder in deionized water and autoclaved at 121 °C for 15 min. A centrifugal-force-driven modular micronozzle device, composed of a modular micronozzle, a micronozzle supporter, and a collection tube, was fabricated as a previously described method to produce microspheres [42]. *C. reinhardtii* was collected by centrifugation at 5000 rpm for 10 min, and then the cell pellet was resuspended in 5 % (w/v) sodium alginate solution at a final concentration of 5×10^7 microalgae/mL [25]. The *C. reinhardtii*-alginate mixture was extruded through the micronozzle with a 25-gauge syringe needle into $CaCl_2$ solution during centrifugation at 1200 rpm for 4 min (Fig. 3a). The distance between the micronozzle tip and the $CaCl_2$ solution surface was set at 1 cm. The newly formed microspheres were soaked in $CaCl_2$ solution for 5 min and then rinsed trice with TAP medium to remove the residual $CaCl_2$. Finally, *C. reinhardtii* alginate microspheres (CAMs) were collected by cell strainers and incubated in fresh TAP medium under 25 °C with continuous illumination for further use. Meanwhile, pure alginate microspheres (AMs) were prepared similarly, except that the alginate solution did not contain microalgae. Bright-field and fluorescent images of CAMs were taken under a confocal laser scanning microscope (CLSM; ZEISS LSM 900 with Airyscan 2, Carl Zeiss Microscopy, Jena, Germany). The diameters of microspheres were measured from bright-field images captured by a digital camera (Nikon, Tokyo, Japan) coupled to a microscope.

2.3. Synthesis of GelMA

The GelMA hydrogel was synthesized following a previously reported method with minor modifications [43]. In brief, 10 % (w/v) type A gelatin from porcine skin (Sigma-Aldrich) was dissolved into Dulbecco's phosphate-buffered saline (DPBS, Sigma-Aldrich) under stirring at 50 °C for 1 h. Then, 8 % (v/v) methacrylic anhydride (Sigma-Aldrich) was added dropwise to the gelatin solution at 50 °C. After stirring for 2 h, the mixture was diluted with an equal volume of preheated DPBS to stop the reaction and then dialyzed against distilled water at 50 °C for 7 days using a 12–14 kDa dialysis membrane (Spectrum Labs, Piscataway, NJ, USA). Finally, the mixture was filtered through a 0.22 μm filter and temporarily stored at −80 °C, followed by lyophilization for 5 days to form porous white foam, and then, the GelMA was stored at −20 °C until further use.

2.4. Encapsulation of DPSCs and alginate microspheres in GelMA hydrogel

5 % (w/v) lyophilized GelMA was dissolved in αMEM containing 0.25 % (w/v) lithium phenyl-2, 4, 6-trimethylbenzoylphosphinate (LAP; Engineering for Life, Suzhou, China) as the photoinitiator at 55 °C. After digestion and centrifugation, DPSCs were resuspended with the precursor GelMA hydrogel solution at the final density of 3×10^6 cells/mL and then mixed with 0.03 g/mL alginate microspheres with or without *C. reinhardtii*. 450 μL of the pre-hydrogel mixture was carefully pipetted to 24-well plates, followed by photo-crosslink using a 405 nm ultraviolet light (Engineering for Life) for 30 s. After gelation, the three-dimensional (3D) hydrogels were cultured in the coculture medium under normoxia for 2 days and then kept under hypoxic conditions for an additional 7 days. Throughout this culture period, the hydrogels were continuously exposed to white light (4500 lux). To visualize cell distribution within GelMA hydrogel under CLSM, the cell-laden scaffolds were incubated in αMEM containing 10 μM CellTracker™ Green CMFDA (Thermo Fisher Scientific) for 30 min to stain live DPSCs, and *C. reinhardtii* was detected by exploiting the red autofluorescence of chlorophyll.

2.5. Oxygen release measurements

The SDR SensorDish® Reader (SDR; PreSens, Regensburg, Germany) was employed to detect dissolved oxygen concentrations following the manufacturer's instructions. In detail, for microalgal oxygen measurements, *C. reinhardtii* was cultured in air-tight PSt5 SensorVials (PreSens) overnight in darkness to remove dissolved oxygen. The SensorVials were then placed on the SDR and exposed to white light (4500 lux), and dissolved oxygen concentrations were recorded at different time points. For coculture system oxygen monitoring, DPSCs were seeded onto 24-well OxoDishes® (PreSens) and indirectly cocultured with *C. reinhardtii*, or different GelMA hydrogels were cultured in 24-well OxoDishes®. Subsequently, the dishes were positioned on the SDR, and the oxygen concentration in the coculture medium was monitored for a 7-day culture period using the SDR software.

2.6. Intracellular hypoxia analysis

For hypoxia-inducible factor-1α (HIF-1α) quantification, DPSCs were incubated in normoxic or hypoxic conditions in the presence of light for 24 h. Total protein was extracted from the cells using a radioimmunoprecipitation assay lysis buffer supplemented with 1 % (v/v) protease inhibitor cocktail (Thermo Fisher Scientific), and the protein concentration was determined by a bicinchoninic acid protein assay kit (Cwbio, Beijing, China). Equivalent amounts of protein lysates were separated by 4–20 % sodium dodecyl sulfate polyacrylamide gel (Beyotime, Shanghai, China) and transferred onto polyvinylidene fluoride membranes. Then, the membranes were blocked with 5 % (w/v) non-fat milk for 1 h at room temperature and incubated overnight at 4 °C with the following primary antibodies: monoclonal mouse anti–HIF–1α (1:500, BD Biosciences, New Jersey, USA), monoclonal mouse anti-α-tubulin (1:2000, Sigma-Aldrich), and monoclonal mouse anti-β-actin (1:1000, Santa Cruz Biotechnology, Santa Cruz, CA, USA). After incubation with horseradish peroxidase-linked anti-mouse secondary antibody (1:1000, Cell Signaling Technology, Danvers, MA, USA) at room temperature for 1 h, the protein bands were visualized using Pierce ECL western blotting substrate (Thermo Fisher Scientific) and quantified by ImageJ software (NIH, Bethesda, MD, USA).

For hypoxyprobe immunofluorescence staining, DPSCs were incubated under normoxic or hypoxic conditions with continuous illumination for 24 h. Next, 5 μM Image-iT Green Hypoxia Reagent (Thermo Fisher Scientific) was added to the culture medium, and the incubation continued for an additional 3 h.

2.7. Detection of ROS

2′,7′-Dichlorodihydrofluorescein diacetate (DCFH-DA; Beyotime) was used as a probe to indicate intracellular ROS production. In detail, DPSCs were cultured with or without *C. reinhardtii* in the presence of light for 24 h. Afterward, cells were incubated in αMEM containing 5 μM DCFH-DA and 2 μg/mL Hoechst for 15 min, rinsed trice with PBS, and imaged under a fluorescence microscope.

2.8. Detection of superoxide dismutase (SOD) activity

The activity of SOD in DPSCs was assessed using a Total Superoxide Dismutase Assay Kit with WST-8 (Beyotime) according to the manufacturer's instructions. Briefly, DPSCs were cultured with or without *C. reinhardtii* in the presence of light. After incubation for 24 h, DPSCs were lysed and centrifuged at 12,000 g for 5 min. The obtained supernatants were utilized for SOD enzymatic activity analysis, with the activity expressed as units per milligram of protein.

2.9. Scanning electron microscopy (SEM)

Alginate microspheres were fixed with 2.5 % (w/v) glutaraldehyde

in PBS overnight at 4 °C and dehydrated with graded ethanol, then air-dried and sputtered with gold by a Magnetron sputter coater (MSP-2S System, Hitachi, Tokyo, Japan). A voltage of 15 kV was used for the SEM analysis (Hitachi). The GelMA hydrogels were lyophilized overnight and were carefully broken to expose their cross-sections. The inner surfaces were sputter-coated with gold, and their microstructure and porosity were characterized by SEM.

2.10. DPSC metabolic activity and viability assays

The metabolic activity of DPSCs indirectly cocultured with *C. reinhardtii* in 2D under constant illumination was determined by Cell Counting Kit-8 (CCK-8; Dojindo, Kumamoto, Japan) according to the manufacturer's protocol. Briefly, at time points 1, 4, and 7 days, transwells were removed, then the coculture medium was replaced by 500 μL of fresh medium containing 50 μL of CCK-8 reagent per well. After incubation for 3 h at 37 °C, the absorbance was measured at 450 nm using a SpectraMax M2 microplate reader (Molecular Devices, Sunnyvale, CA, USA).

To assess the cellular metabolism of DPSCs co-encapsulated with alginate microspheres in 3D GelMA hydrogel under constant light exposure, a Neutral Red Assay (Abcam, Cambridge, UK) was performed as directed by the instructions. In brief, on 1, 4, and 7 days, the culture medium was removed and replaced by 600 μL of neutral red staining solution per well. After incubation for 3 h at 37 °C, the staining solution was removed and replaced by 600 μL of solubilization solution per well. After incubation for 1 h on a shaker at room temperature, the absorbance was measured at 540 nm using a microplate reader.

The viability of DPSCs was evaluated using the Live/Dead/Viability/Cytotoxicity Kit (Thermo Fisher Scientific). Samples were rinsed with PBS and incubated in a fresh medium containing 4 μM ethidium homodimer-1 and 2 μM calcein acetoxymethyl for 30 min at 37 °C. After imaging with CLSM, quantification of live and dead cells was performed using ImageJ software, and cell viability was defined as the ratio of the number of live cells to the total number of cells. The live/dead experiments were performed in triplicate, and three images were randomly obtained for each sample.

2.11. Growth and viability of immobilized microalgae

At certain time points, CAMs were dissolved in 0.9 % (w/v) NaCl solution containing 55 mM sodium citrate (Sigma-Aldrich) for 10 min to recover microalgae from the alginate matrix. *C. reinhardtii* was subsequently collected by centrifugation at 5000 rpm for 10 min, and the pellet was resuspended in the same volume of TAP medium. Then, the optical density (OD) was spectrophotometrically read at 750 nm using a microplate reader to determine *C. reinhardtii* growth.

To evaluate the viability of *C. reinhardtii* in alginate microspheres, live/dead imaging was performed [44]. Briefly, CAMs were incubated in TAP medium containing 5 μM SYTOX Green Dead Cell Stain (Thermo Fisher Scientific) for 10 min at room temperature and then imaged under a CLSM. The SYTOX dye penetrated damaged cell membranes and stained dead microalgae green, whereas viable microalgae were visualized utilizing the red autofluorescence of chlorophyll.

2.12. Adenosine triphosphate (ATP) measurements

To determine intracellular ATP levels, an Enhanced ATP Assay Kit (Beyotime) was used following the manufacturer's instructions. In detail, DPSCs were cultivated under hypoxic conditions and exposed to light for 24 h in the presence or absence of *C. reinhardtii*. Subsequently, the cells were lysed and centrifuged to obtain the supernatant. The detecting solution was added to a 96-well opaque plate and incubated at room temperature for 5 min. Then, the supernatants were introduced into wells and mixed quickly before detecting the luminescence signals by a microplate reader in luminescent mode.

2.13. Bacterial culture

Porphyromonas gingivalis (*P. gingivalis*, ATCC 33277), *Fusobacterium nucleatum* (*F. nucleatum*, ATCC 10953), and *Streptococcus gordonii* (*S. gordonii*, ATCC 10558), were acquired from the American Type Culture Collection (ATCC). *P. gingivalis* and *F. nucleatum* were cultivated in Pg broth (Sigma-Aldrich) supplemented with 1 % (v/v) hemin/vitamin K, and *S. gordonii* was cultured in Brain-Heart Infusion (BHI) broth (Sigma-Aldrich). The culture was performed in an anaerobic chamber (85 % N_2, 10 % H_2, 5 % CO_2) at 37 °C.

2.14. Antibacterial activity of photosynthetic hydrogel

A volume of 1 mL microbial suspension of *P. gingivalis* (10^7 colony forming units (CFU)/mL), *F. nucleatum* (10^7 CFU/mL), and *S. gordonii* (10^5 CFU/mL) were individually added into 24-well plates filled with different GelMA hydrogels and incubated at 37 °C in an anaerobic chamber with continuous illumination (4500 lux). Afterward, the bacterial growth was quantified by measuring their absorbance at 660 nm. Meanwhile, bacterial suspension was spread on the Columbia blood agar plates. After 3 days, the colonies on the blood agar plates were imaged and calculated to evaluate bacteria viability. To detect ROS content in bacteria, a volume of 1 mL polymicrobial suspension was added to 24-well plates and incubated with GelMA hydrogels under white light exposure for 24 h, and then the DCFH-DA fluorescent probe was used, as previously mentioned in section 2.7.

2.15. Antibiofilm effects of photosynthetic hydrogel

To investigate the efficacy of photosynthetic hydrogel in preventing biofilm formation, multispecies biofilms were established with slight modifications based on prior studies [45,46]. Briefly, 10^8 CFU/mL *P. gingivalis*, 10^8 CFU/mL *F. nucleatum*, and 10^7 CFU/mL *S. gordonii* were mixed in a ratio of 1:1:1 to form a polymicrobial suspension. Then, the suspension was inoculated onto 24-well plates containing GelMA hydrogels with round glass climbing slices on the surface. The plates were incubated in an anaerobic chamber with continuous illumination for 72 h. Following biofilm formation, the biofilms were stained with 2.5 μM SYTO 9 and 2.5 μM propidium iodide (Live/Dead BacLight Bacterial Viability Kit, Thermo Fisher Scientific) for 30 min. Then, the bacteria's viability and biofilms' thickness were assessed using CLSM. To further analyze the biofilm surface topography, the biofilms were fixed in 2.5 % (w/v) glutaraldehyde, dehydrated with graded ethanol, and observed under SEM.

To assess the efficacy of eradicating mature biofilms, the polymicrobial suspension previously described was inoculated onto 24-well plates with round glass climbing slices on the bottom of each well and allowed to form multispecies biofilms for 72 h in an anaerobic chamber. The biofilms were then treated with various GelMA hydrogels for an additional 24 h under constant illumination. Similarly, the morphology, viability, and thickness were evaluated using SEM and CLSM, respectively. Also, the hypoxic status of biofilms was visualized using the hypoxyprobe, as mentioned in section 2.6.

2.16. Statistical analysis

All experiments were performed at least three times independently. Data were presented as mean ± standard deviation (SD). A two-tailed Student's *t*-test was performed to evaluate the differences between the two groups. One-way ANOVA and two-way ANOVA with Tukey's post hoc test were used for multiple comparisons. $P < 0.05$ was considered statistically significant. All statistical analyses were performed using the GraphPad Prism 6 software (San Diego, CA, USA).

3. Results and discussion

3.1. Photosynthetic activity and biocompatibility of C. reinhardtii

C. reinhardtii, a unicellular green microalga with a spherical morphology, emitted red autofluorescence due to the presence of chlorophyll (Fig. 1a and b). *C. reinhardtii* was exposed to white light to validate its oxygen generation capacity, and the dissolved oxygen concentration was monitored using an oxygen meter. As expected, the generated oxygen was positively correlated with algal concentrations at both 25 °C and 37 °C (Fig. 1c). Under illumination, the dissolved oxygen concentration increased gradually within 30 min, while in the absence of light, it decreased (Fig. 1d). The oxygenation profiles displayed similar trends across three cycles of light and dark exposure at both 25 °C and 37 °C, indicating that photosynthesis is shut off when light is absent. As shown in Fig. 1e, the dissolved oxygen concentration at 37 °C was lower than that at 25 °C. Furthermore, a gradual decline was observed after 2 days. This could be partially ascribed to the fact that 37 °C is suitable for mammalian cell culture but may be unfavorable for the growth and photosynthesis of *C. reinhardtii*. Thus, further studies should be conducted to explore other thermotolerant microalgae strains or cyanobacteria. These findings confirm that the oxygen production capacity of *C. reinhardtii* depends on its concentration, light exposure, and environment temperature, and therefore, oxygen tensions required by various cells and tissues could be adjusted by modifying such parameters. We subsequently studied the biocompatibility of *C. reinhardtii* using the CCK-8 assay. DPSCs were cocultured with gradient concentrations of *C. reinhardtii* for 4 days under normoxic or hypoxic conditions in the presence of light. As depicted in Fig. 1f and g, the proliferation of DPSCs cocultured with *C. reinhardtii* was significantly higher than that of the control group under both normoxia or hypoxia, indicating no apparent cytotoxicity of *C. reinhardtii* towards DPSCs. These results suggest that *C. reinhardtii* possesses outstanding photosynthetic activity and favorable biocompatibility.

3.2. Photosynthetic oxygen produced by C. reinhardtii improves DPSC survival under hypoxia

Oxygen is a fundamental molecule for cell survival, physiological functions, and differentiation [47]. DPSCs, a promising population of mesenchymal stem cells, possess high proliferative and multipotent differentiation potentials in various tissue regenerations, including oral, bone, cartilage, adipose, neural, and vascular tissues [48]. To investigate the effects of oxygen supplied by *C. reinhardtii* through photosynthesis on DPSCs, an indirect coculture system was established (Fig. 2a), allowing gas exchange without direct contact between cells and microalgae. The dissolved oxygen concentrations in the coculture medium were monitored for 7 days. Under hypoxia, when DPSCs were cocultured with *C. reinhardtii* in the presence of light, the oxygen concentration displayed a stable increase over time, reaching approximately 9.63 mg/L within the first 2 days, followed by a downward trend, reaching 6.45 mg/L after 4 days and 3.37 mg/L after 7 days (Fig. 2b). This observation can be primarily attributed to the fact that 37 °C is not an optimal temperature for *C. reinhardtii* photosynthesis, consistent with the findings in Fig. 1e. Next, a hypoxyprobe Image-iT (green) was employed to determine if this photosynthetic oxygen could alleviate DPSC intracellular hypoxia. As illustrated in Fig. 2c, bright green fluorescence was observed in DPSCs without *C. reinhardtii*, while faint green fluorescence was detected when cocultured with *C. reinhardtii* under hypoxia, with similar intensity to the normoxia group. HIF-1α, a key transcription factor mediating cellular adaptive response to hypoxia, was significantly upregulated in DPSCs under hypoxia compared to normoxia, with an approximately 2-fold increase in protein expression. Interestingly, HIF-1α was substantially downregulated in the presence of *C. reinhardtii*, exhibiting a similar expression level as in normoxia (Fig. 2d and e). These findings confirm that *C. reinhardtii* can deliver sustained and sufficient oxygen through photosynthesis to relieve intracellular hypoxic conditions. One concern regarding oxygen supply is ROS overproduction, which is detrimental to cell survival. The generation of ROS induced by *C. reinhardtii* was determined using DCFH-DA staining. As depicted in Fig. S1, all three groups exhibited similar low-intensity green fluorescence signals, indicating that photosynthesis-derived oxygen did not significantly increase the total intracellular ROS levels. The previous study demonstrated that high oxygen pressure favored the production of ROS; however, cells can develop antioxidant enzymes to eliminate excess ROS and avoid oxidative stress [49]. Therefore, we further evaluated the enzymatic activity of SOD, a crucial endogenous antioxidant enzyme, to investigate the response of DPSCs to the oxygen produced by *C. reinhardtii*. As shown in Fig. S2, SOD activity in DPSCs cocultured with *C. reinhardtii* under hypoxia was significantly higher than that in the hypoxia group, reaching levels comparable to the normoxia group. These results suggest that when DPSCs were exposed to an appropriately oxygen-rich microenvironment, they could enhance the activity of endogenous antioxidant enzymes to scavenge excessive ROS, thereby restoring cellular redox homeostasis. Taken together, these findings indicate that photosynthetic oxygen did not induce oxidative stress damage in DPSCs. Subsequently, to evaluate whether oxygen released by *C. reinhardtii* improves cell survival under hypoxia, the coculture system was placed in a hypoxic chamber with constant illumination for 7 days. Results revealed that hypoxia inhibited the metabolic activity of DPSCs in monoculture over time. In contrast, coculture with *C. reinhardtii* significantly improved cellular metabolism on days 4 and 7 (Fig. 2f). Cell viability, assessed by live/dead staining assay, showed only 70 % viable cells in monoculture after 4 days, while coculture maintained a survival ratio of around 90 % (Fig. 2g and h). These findings are consistent with a recent study reporting that photosynthetic cyanobacteria can produce oxygen to enhance cell survival and proliferation of lymphatic endothelial cells [50]. Furthermore, intracellular ATP concentration measurements demonstrated that, in the absence of *C. reinhardtii*, DPSCs produced only 13 μM under hypoxia, while ATP production in DPSCs cocultured with *C. reinhardtii* elevated remarkably to 19 μM (Fig. 2i). This result could be attributed to the adequate oxygen supply by *C. reinhardtii*, enabling aerobic metabolism of glucose to generate abundant ATP for various physiological processes [51]. Collectively, these results support our hypothesis that *C. reinhardtii* can release sufficient oxygen upon illumination to reverse cellular hypoxia and improve energy production under hypoxic conditions, thereby facilitating metabolic activity and viability of DPSCs.

3.3. Preparation and characterization of C. reinhardtii alginate microspheres

To maintain microalgae in position and minimize potential immune responses, *C. reinhardtii* (5×10^7 microalgae/mL) was immobilized in alginate microspheres, as described in section 2.2 (Fig. 3a). A previous study reported that photosynthetic hydrogels demonstrated optimal oxygen production capacity at 5×10^7 microalgae/mL among concentrations ranging from 1×10^7 to 2.5×10^8 microalgae/mL [25]. Even though more oxygen production might be expected with more microalgae, this surprising result could be due to higher oxygen consumption and a stronger self-shading effect at higher microalgae densities [52]. Fig. 3b, c illustrate well-shaped spherical alginate microspheres with an average diameter of 452.8 μm. Bright-field and fluorescence images display the homogeneous distribution of *C. reinhardtii* in alginate microspheres (Fig. 3d and e). Additionally, the external surface morphology and internal structure of alginate microspheres were analyzed by SEM. As shown in Fig. 3f and g, the external surface of both microsphere types appeared wrinkled. The internal surface of AMs was smooth, in contrast to the rough internal surface observed in CAMs (Fig. 3h and i). Altogether, these images prove the successful incorporation of microalgae into alginate microspheres. Unlike the

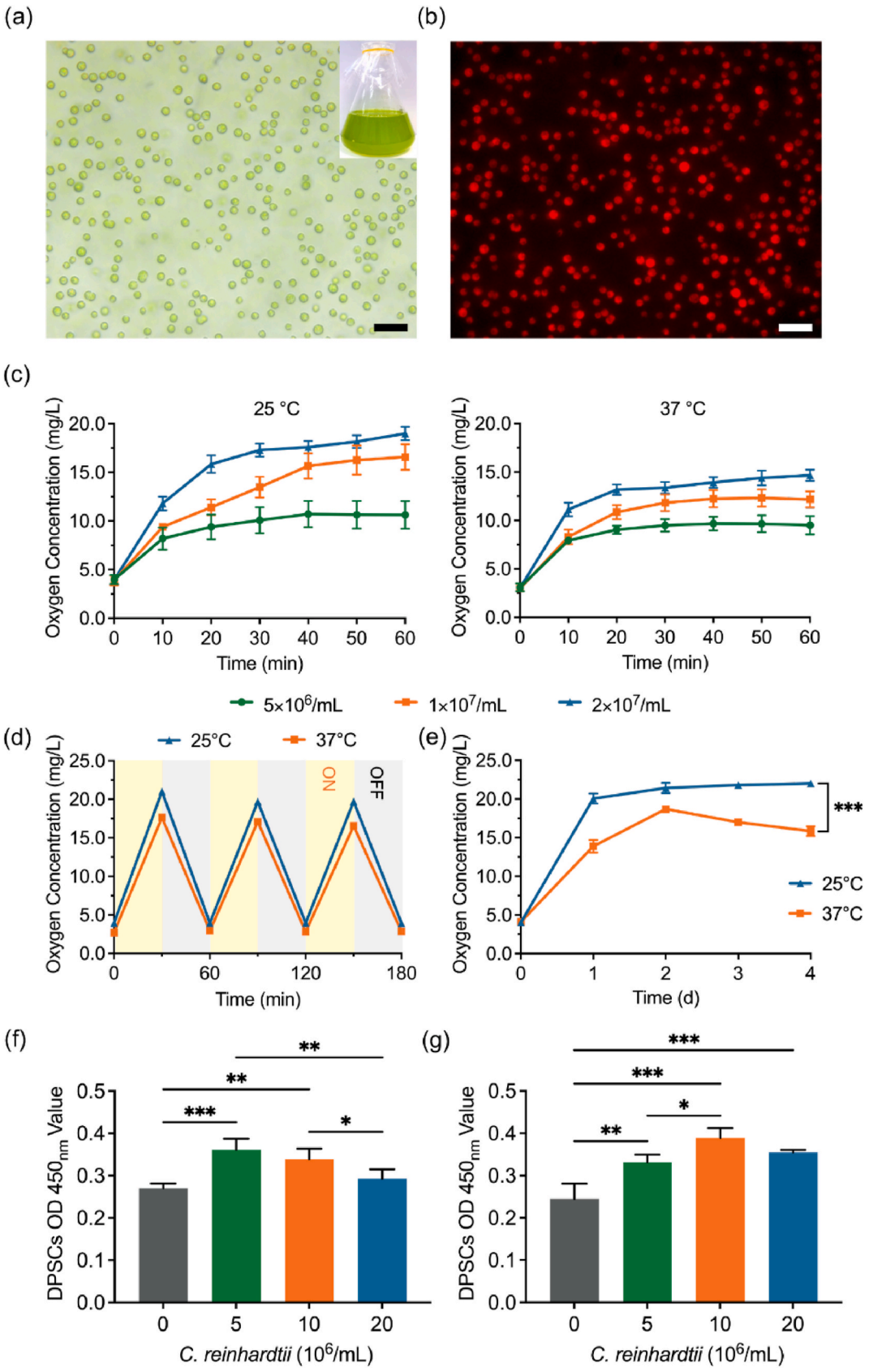

Fig. 1. Characterization of *C. reinhardtii*. (a) Bright-field and (b) fluorescence images of *C. reinhardtii*. Inset: large-scale culture of microalgae. (c) Dissolved oxygen produced by *C. reinhardtii* at different concentrations under light conditions at 25 °C and 37 °C. (d) Dissolved oxygen released by *C. reinhardtii* under light (ON, yellow) and dark (OFF, gray) conditions at 25 °C and 37 °C. (e) Comparison of the photosynthetic activity of *C. reinhardtii* at 25 °C and 37 °C. Proliferation of DPSCs cocultured with different concentrations of *C. reinhardtii* under (f) normoxic and (g) hypoxic conditions. Scale bars: 25 μm (a, b). $*p < 0.05$, $**p < 0.01$, $***p < 0.001$. (For interpretation of the references to color in this figure legend, the reader is referred to the Web version of this article.)

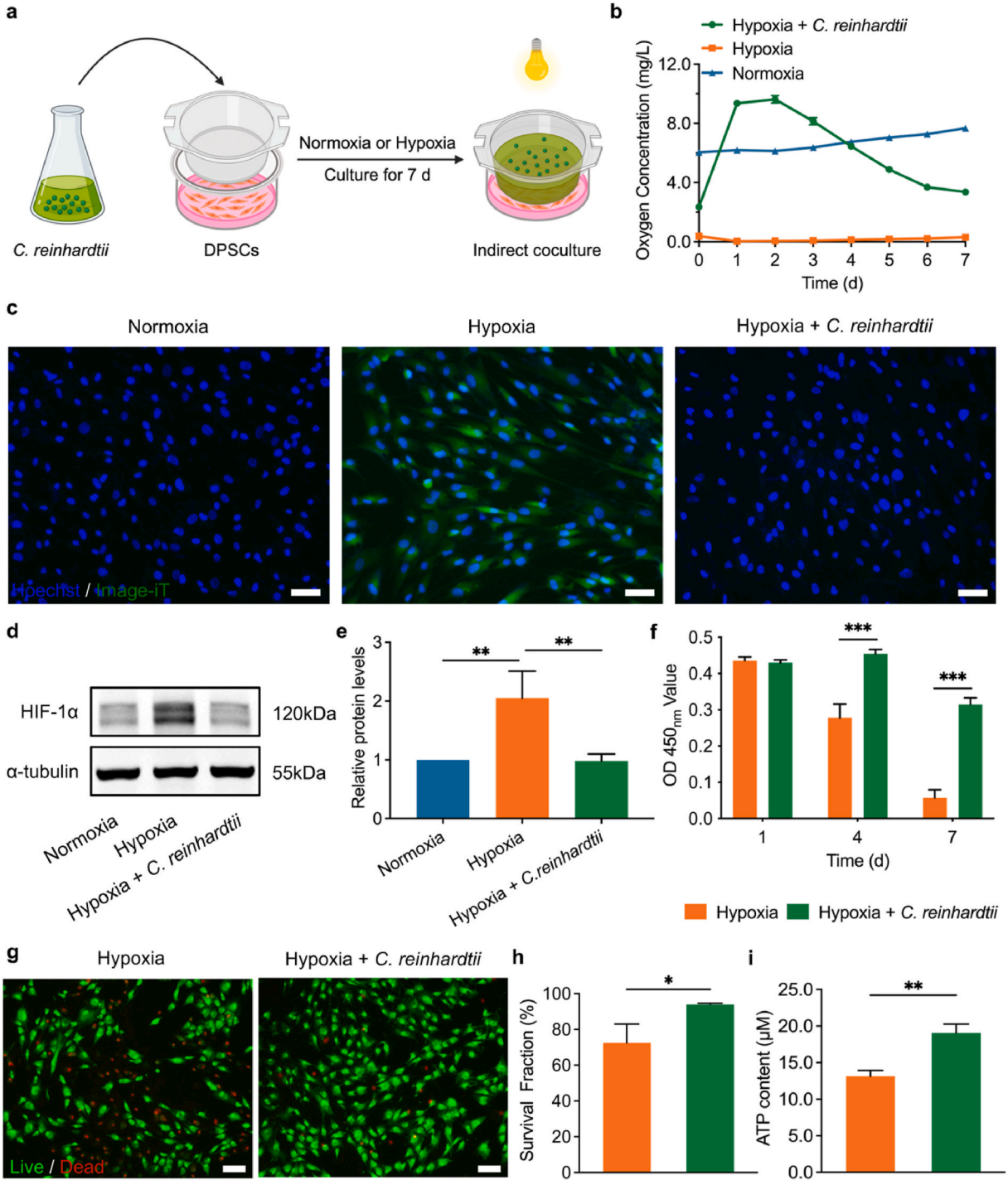

Fig. 2. Photosynthetic oxygen produced by *C. reinhardtii* improves DPSC survival under hypoxia. (a) Schematic illustration of the indirect coculture of DPSCs and *C. reinhardtii*. (b) Dissolved oxygen concentrations in the coculture medium of DPSCs incubated under different conditions. (c) Representative fluorescence images of DPSCs stained with Hypoxyprobe Image-iT (green) and Hoechst (blue) under different conditions. (d) Western blotting images and (e) corresponding quantification of HIF-1α expression in DPSCs after 24 h of different treatments. (f) Metabolic activity of DPSCs cultured with or without *C. reinhardtii* under hypoxia for 7 days. (g) Representative fluorescence images of live/dead staining and (h) corresponding quantification of the survival fraction of DPSCs cultured with or without *C. reinhardtii* under hypoxia for 4 days. (i) Intracellular ATP content in DPSCs cultured with or without *C. reinhardtii* under hypoxia for 24 h. Scale bars: 50 μm (c), 100 μm (g). $^{*}p < 0.05$, $^{**}p < 0.01$, $^{***}p < 0.001$. (For interpretation of the references to color in this figure legend, the reader is referred to the Web version of this article.)

sophisticated pump-based microfluidic devices, the centrifugal-force-driven modular micronozzle device utilized in this study is cost-effective and conveniently operated, enabling the mass production of microspheres within a few minutes [42].

Following the successful fabrication of CAMs, we further evaluated the growth, viability, and photosynthetic activity of immobilized *C. reinhardtii*. *C. reinhardtii* was initially encapsulated at a low concentration (1×10^7 microalgae/mL) to assess microalgae proliferation. As shown in Fig. 3j, the macroscopic images captured over time, CAMs appeared nearly colorless on day 1 and gradually turned dark green after 14 days of incubation at 25 °C with light irradiation. Simultaneously, the cell density of *C. reinhardtii* was verified by measuring OD values at 750

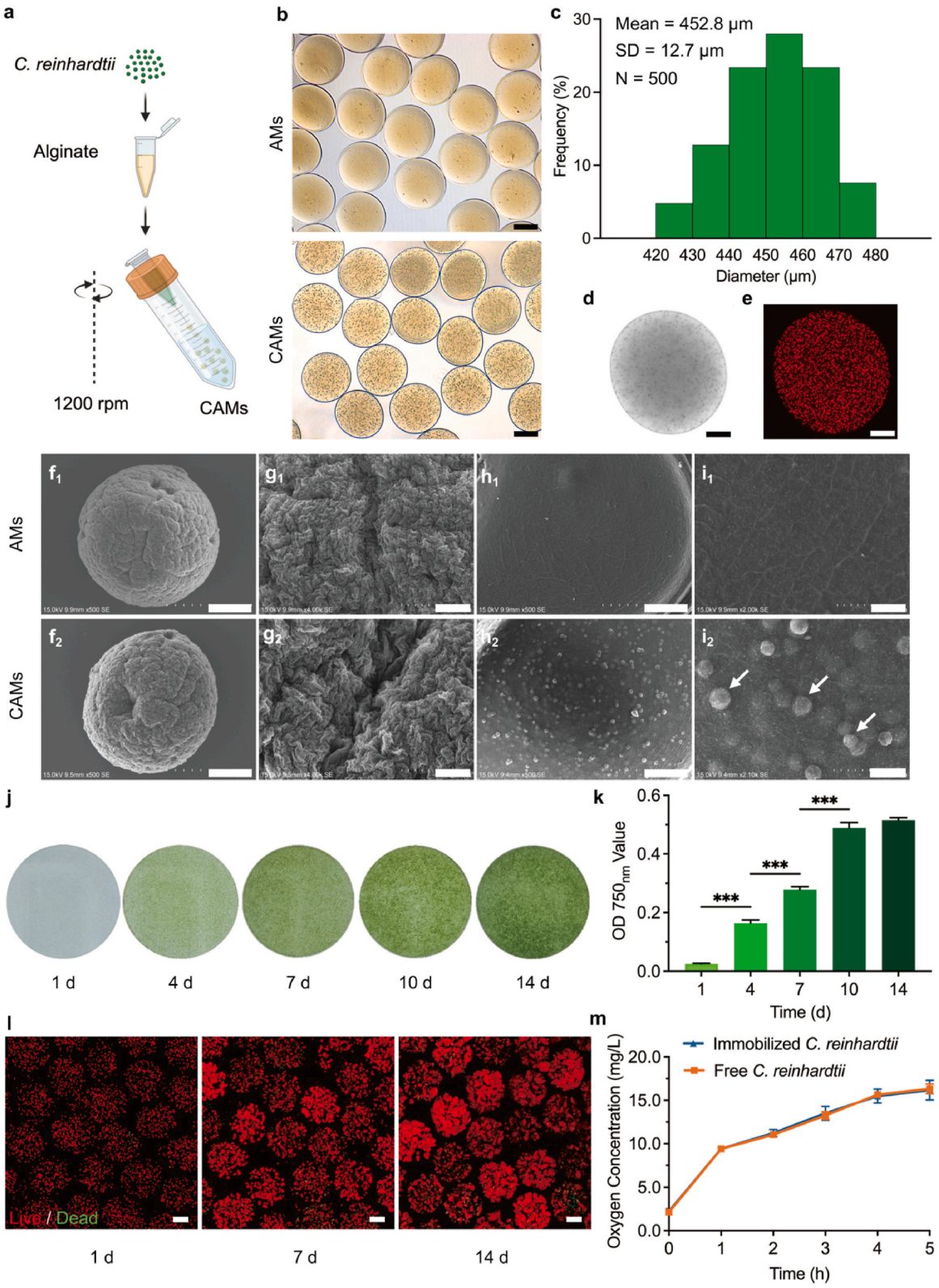

Fig. 3. Characterization of *C. reinhardtii* alginate microspheres (CAMs). (a) Schematic illustration of the immobilization of *C. reinhardtii* in alginate microspheres. (b) Bright-field images and (c) diameter distribution of alginate microspheres. (d) Representative bright-field and (e) fluorescence images of CAMs. (f, g) Representative SEM images of the external surface and (h, i) internal structure of alginate microspheres. White arrows indicate *C. reinhardtii*. (j) Macroscopic images of CAMs incubated for 14 days. (k) Cell density of *C. reinhardtii* in alginate microspheres. (l) Representative fluorescence images of live/dead staining for *C. reinhardtii* immobilized in alginate microspheres. (m) Comparison of the oxygen-producing capability of immobilized and free *C. reinhardtii*. Scale bars: 5 μm (g), 10 μm (i), 50 μm (f, h), 100 μm (d, e), 200 μm (b, l). ***$p < 0.001$.

nm, revealing a steady increase over the culture period (Fig. 3k). Additionally, live/dead staining intuitively illustrated that most microalgae in alginate microspheres remained viable, and proliferated to form clusters after 14 days of cultivation (Fig. 3l). Next, the oxygen-producing capability of CAMs was determined. As depicted in Fig. 3m, the dissolved oxygen concentration produced by immobilized *C. reinhardtii* gradually increased from 2.24 to 16.17 mg/L within 5 h, comparable to free *C. reinhardtii*. This result indicates that *C. reinhardtii* can maintain equivalent photosynthetic activity with or without alginate encapsulation. Our findings agree with the previous studies highlighting the general suitability of alginate for microalgae immobilization [53,54]. Various materials have also been utilized for microalgae entrapment, including GelMA [55], collagen [50], silk fibroin [56], and chitosan [57]. Among these, sodium alginate is the preferred natural polymer for immobilization due to its ease of handling, biocompatibility, biodegradability, high transparency, and nutrient availability [58]. The advantages of immobilization include the shielding effect of hydrogels, such as retardation of external substance diffusion and partial absorption of shear forces [58]. In a nutshell, alginate microspheres serve as a "cage" that not only fixes *C. reinhardtii* but also protects them from extreme changes in the physicochemical environment, enabling them to remain viable and photosynthetically active.

3.4. Fabrication and characterization of photosynthetic GelMA hydrogel

GelMA hydrogels are extensively employed in regenerative medicine due to their favorable biological properties and adjustable physical characteristics, including biocompatibility, biodegradability, transparency, permeability, and photo-crosslinking [59]. They closely mimic the native extracellular matrix, allowing cell attachment, spreading, proliferation, and differentiation. However, oxygen availability poses a critical challenge in tissue engineering, as inner regions of 3D scaffolds often suffer from oxygen deprivation due to limited diffusion and lack of vasculature [60,61]. Although transplanted cells can withstand transient and mild hypoxia, prolonged and severe hypoxia inevitably leads to extensive cell death and impaired regeneration [62]. Motivated by the benefits of photosynthetic oxygenation and enhanced cell survival observed in a 2D coculture of DPSCs and *C. reinhardtii*, we developed a photosynthetic hydrogel for tissue regeneration. The direct co-incorporation of DPSCs and free *C. reinhardtii* within the 3D hydrogel led to significant DPSC death, potentially attributed to the unrestricted growth of *C. reinhardtii*, which competed for space and nutrients with DPSCs (data not shown). To address this issue, in this study, *C. reinhardtii* was initially immobilized in alginate microspheres and then co-encapsulated with DPSCs within GelMA hydrogel. To visualize the distribution of DPSCs and *C. reinhardtii*, 3D fluorescent images were captured using CLSM, revealing a homogeneous distribution of DPSCs and *C. reinhardtii*, with proximity but no direct contact within CAMs@GelMA hydrogel, enabling efficient oxygen delivery while immobilizing microalgae in position (Fig. 4a). The cross-sectional microstructure of different GelMA hydrogels was examined by SEM. As illustrated in Fig. 4b and c, all GelMA hydrogels exhibited a highly porous and interconnected structure (denoted by asterisks) that facilitates oxygen and nutrient transport. The SEM images of the GelMA hydrogel containing AMs (AMs@GelMA) and CAMs (CAMs@GelMA) further confirmed that alginate microspheres (marked by white arrows) were fully encapsulated within the hydrogel matrix without affecting GelMA crosslinking, and *C. reinhardtii* (indicated by green arrows) were effectively immobilized in CAMs. Subsequently, the oxygen concentrations in GelMA hydrogels were monitored for 7 days in a hypoxia incubator. As depicted in Fig. 4d, the oxygen levels in CAMs@GelMA hydrogels decreased slowly over time but remained at 2.56 mg/L for up to 7 days. In contrast, the oxygen concentrations in pure GelMA hydrogels and AMs@GelMA hydrogels were barely above 0 mg/L. This can be attributed to the oxygen consumption by DPSCs during respiration. We further examined whether the oxygen provided by CAMs effectively ameliorated the intracellular hypoxic state of DPSCs. As shown in Fig. 4e and f, the expression of HIF-1α in DPSCs was dramatically downregulated when co-encapsulated with CAMs. Similarly, intense green fluorescence signals were detected in GelMA and AMs@GelMA hydrogels, whereas CAMs@GelMA hydrogels displayed almost no green fluorescence (Fig. 4g). These results demonstrate that the oxygen produced by CAMs through photosynthesis is sufficient to circumvent the hypoxic status of encapsulated cells. Several oxygen-supplying strategies have been proposed to address the hypoxia issue in tissue engineering. For instance, peroxides and sodium percarbonates can generate oxygen via chemical decomposition [16,17]; perfluorocarbon and hemoglobin, as oxygen carriers, can transfer oxygen within biomaterials [14,15]. In comparison, photosynthetic biomaterials offer a consistent and adequate oxygen supply without generating toxic byproducts like H_2O_2 and ROS; photosynthesis consumes metabolic waste, such as CO_2, and its oxygen generation capacity can be modulated by light intensity.

3.5. High survivability of DPSCs within photosynthetic hydrogel under hypoxia

After co-encapsulation of DPSCs and alginate microspheres, the GelMA hydrogels were initially incubated under normoxic conditions for 2 days and transferred to a hypoxia incubator with continuous illumination for a 7-day culture period. To assess the metabolic activity of DPSCs, a neutral red assay was conducted, revealing that DPSCs encapsulated in CAMs@GelMA hydrogels exhibited significantly higher metabolic activity on days 4 and 7 compared to the other groups (Fig. 5a). Next, live/dead staining was employed to visualize cell viability within different GelMA hydrogels. As illustrated in Fig. 5b, the number of dead DPSCs increased over time in GelMA and AMs@GelMA hydrogels, whereas most DPSCs in CAMs@GelMA hydrogels remained viable and exhibited an elongated morphology. Quantitative analysis demonstrated that DPSCs encapsulated in GelMA or AMs@GelMA hydrogels underwent cell death, with approximately 74.7 % and 61.8 % survivability on days 4 and 7, respectively. In contrast, DPSCs within CAMs@GelMA hydrogels maintained consistently higher survival rates of 85.9 % and 85.5 % after 4 and 7 days, compared to the other groups (Fig. 5c). These findings are consistent with a recent study that reported a symbiotic relationship between mammalian cells and microalgae, wherein the presence of *C. reinhardtii* within the hydrogel enhanced HepG2 cell viability and functionality [27].

3.6. Antibacterial activity of photosynthetic hydrogel

The oral cavity is a complex environment, harboring approximately 700 bacteria species [63]. Among them, anaerobic bacteria thrive in hypoxic microenvironments, resulting in increased inflammation and impaired tissue regeneration [35]. Effective infection control is a prerequisite for tissue repair and regeneration. Oxygen can disrupt hypoxic environments and interfere with anaerobic metabolic pathways [64]. Thus, we hypothesized that photosynthetic hydrogels with local oxygen enrichment could impede anaerobic infections.

S. gordonii is an early colonizer commonly found in dental plaque [65], while *F. nucleatum* acts as a bridge colonizer in plaque and periodontitis, connecting early and late colonizers [66]. *P. gingivalis*, a late colonizer, is widely recognized as a key pathogen in the occurrence and progression of periodontitis [67]. Therefore, *S. gordonii*, *F. nucleatum*, and *P. gingivalis* were selected as representative oral bacteria models to investigate the antibacterial activity of the photosynthetic hydrogel. First, bacterial growth was evaluated by measuring the OD values at 660 nm of bacterial suspension treated with different GelMA hydrogels. After 6 h of incubation, there were no significant differences in the growth of *P. gingivalis*, *F. nucleatum*, and *S. gordonii* among the three groups (Fig. S3a). However, following 12 h and 24 h of incubation, the CAMs@GelMA hydrogels significantly inhibited the growth of both

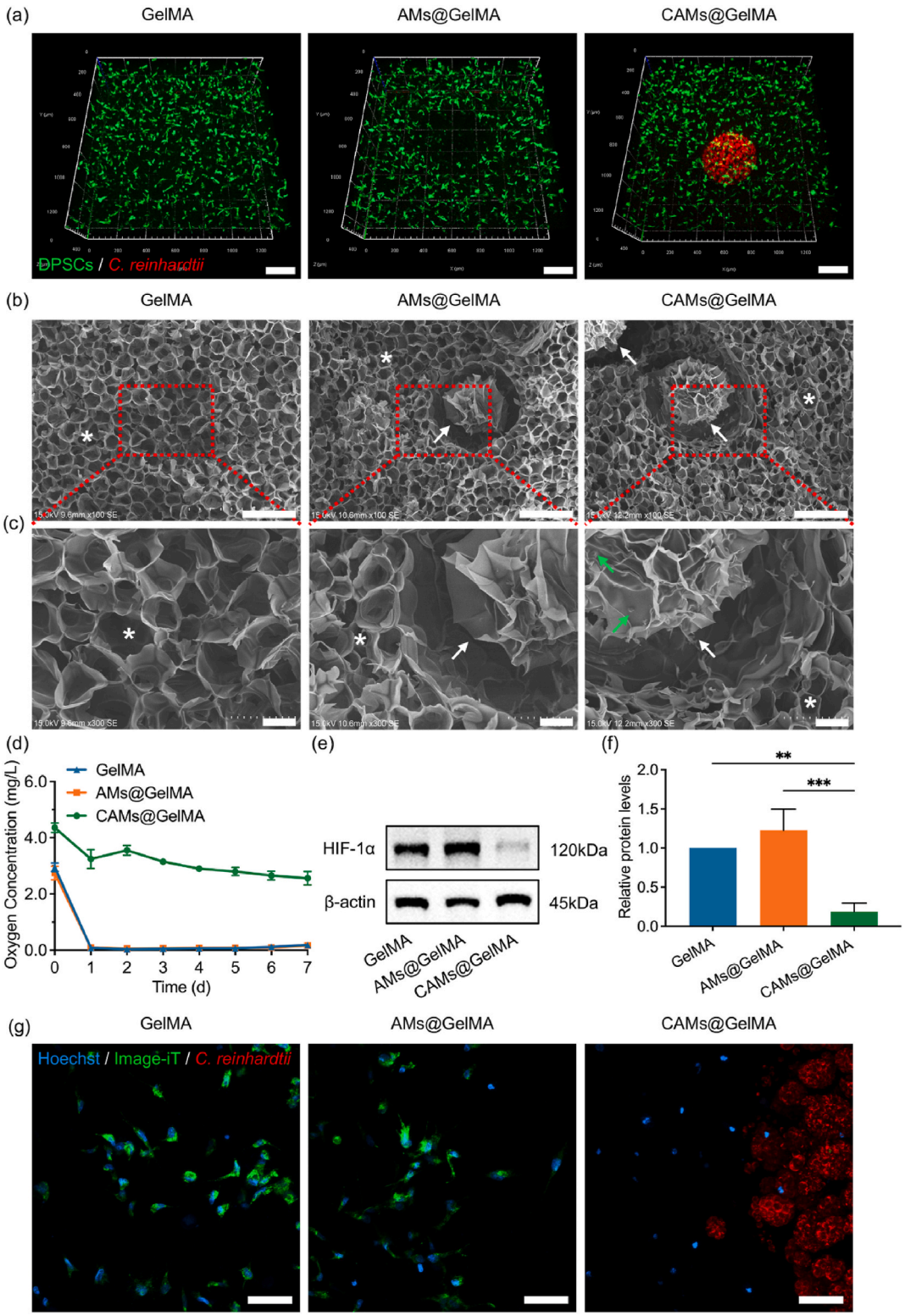

Fig. 4. Characterization of photosynthetic GelMA hydrogel. (a) 3D fluorescent images showing the distribution of DPSCs (green) and *C. reinhardtii* (red) within different GelMA hydrogels. (b, c) Representative SEM images of the inner pore structure of different GelMA hydrogels. Asterisks denote GelMA hydrogels, white arrows point to alginate microspheres, and green arrows indicate immobilized *C. reinhardtii*. (d) Comparison of oxygen concentration in different GelMA hydrogels incubated under hypoxia. (e) Western blotting images and (f) corresponding quantification of HIF-1α expression in DPSCs encapsulated in different GelMA hydrogels for 24 h. (g) Representative fluorescence images of DPSCs stained with Hypoxyprobe Image-iT (green) and Hoechst (blue) within different GelMA hydrogels. Scale bars: 50 μm (c, g), 200 μm (a), 250 μm (b). $^{**}p < 0.01$. $^{***}p < 0.001$. (For interpretation of the references to color in this figure legend, the reader is referred to the Web version of this article.)

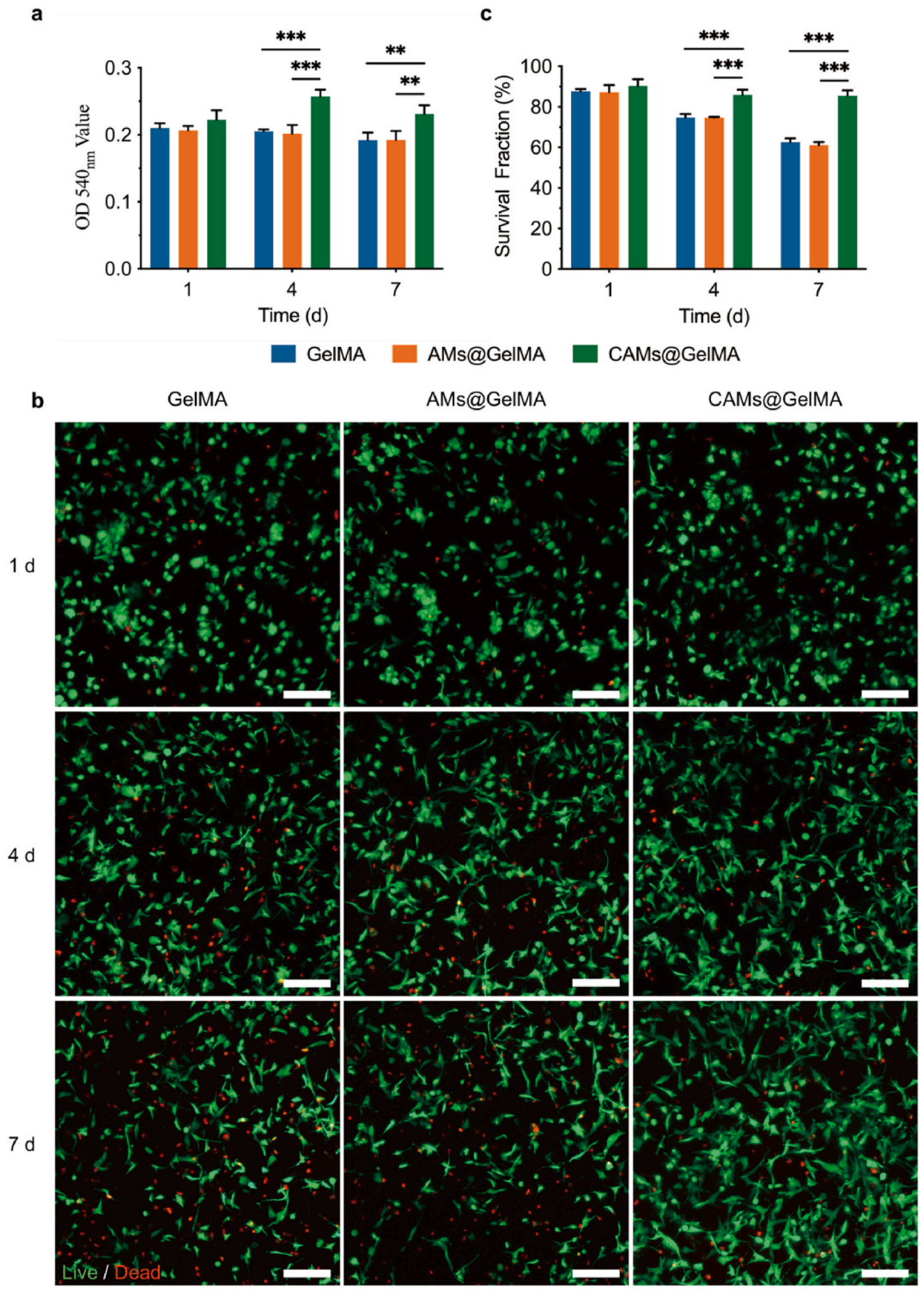

Fig. 5. High survivability of DPSCs within photosynthetic hydrogel under hypoxia. (a) Metabolic activity of DPSCs encapsulated in different GelMA hydrogels under hypoxia for 7 days. (b) Representative fluorescence images of live/dead staining and (c) corresponding quantification of the survival fraction of DPSCs encapsulated in different GelMA hydrogels. Scale bars: 100 μm (b). $^{**}p < 0.01$. $^{***}p < 0.001$.

P. gingivalis and *F. nucleatum*, while no effect was observed on *S. gordonii* (Fig. S3b and Fig. 6a). Subsequently, the CFU counting method was utilized to assess bacterial viability. As illustrated in Fig. 6b and c, after 24 h of treatment with CAMs@GelMA hydrogels, no colony formation of *P. gingivalis* and *F. nucleatum* was observed, in contrast to the dense bacterial colonies seen in the GelMA and AMs@GelMA groups. Similarly, there were no discernible differences in *S. gordonii* colony formation among the three groups. The observed discrepancy can be attributed to the unique characteristics of different bacterial species. *P. gingivalis* and *F. nucleatum* are Gram-negative anaerobes lacking the ability to synthesize a respiratory chain for utilizing oxygen as the final electron acceptor; thus, they are highly susceptible to oxygen toxicity [68]. In contrast, *S. gordonii*, a Gram-positive aerobe, exists as a non-pathogenic commensal in the normal oral microflora [65].

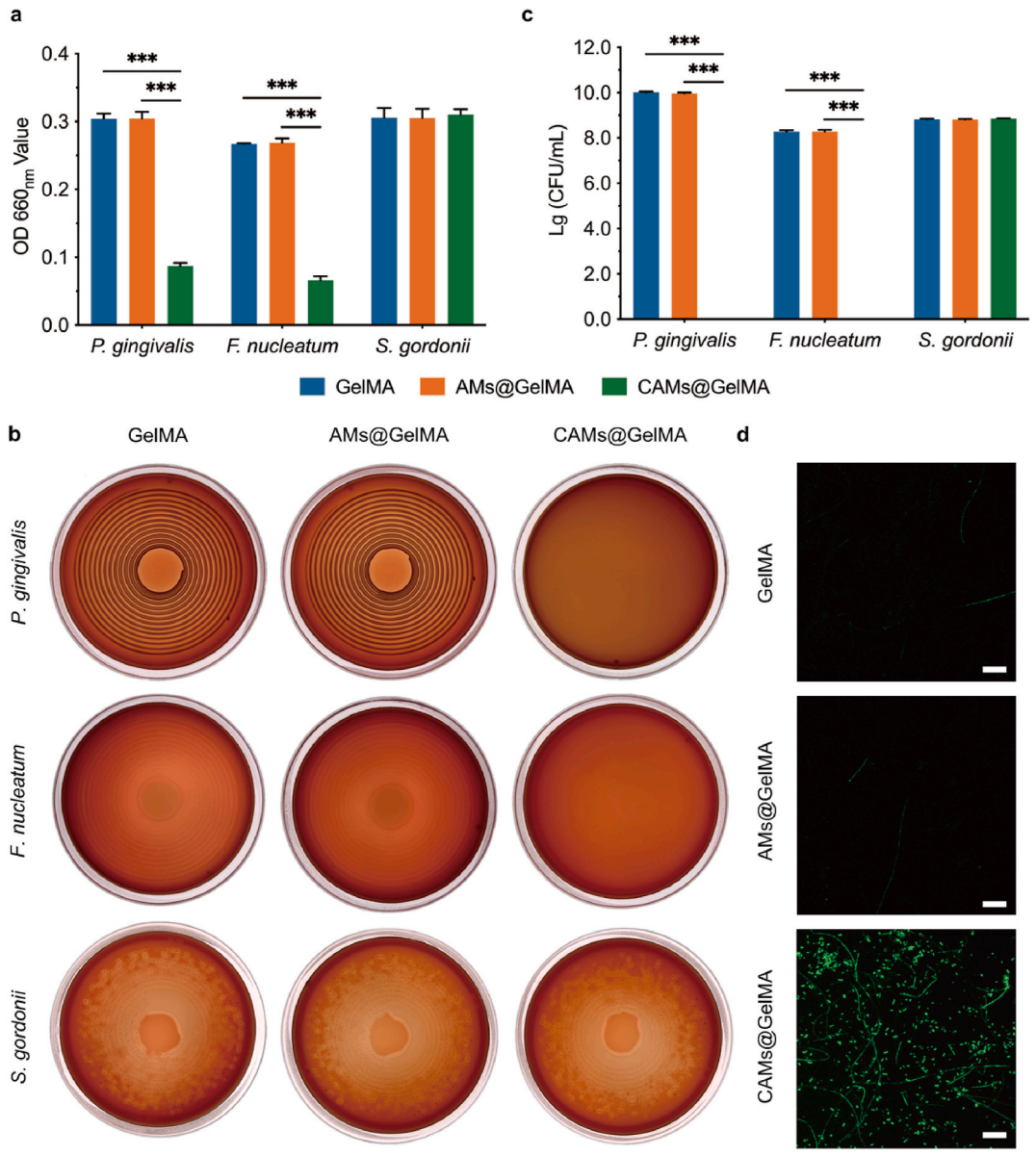

Fig. 6. Antibacterial activity of photosynthetic hydrogel. (a) Antibacterial effects of different GelMA hydrogels on planktonic bacteria after 24 h. (b) Representative CFU images and (c) corresponding colony counts of bacteria treated with different GelMA hydrogels for 24 h. (d) Representative fluorescence images of ROS stained by DCFH-DA (green) in multi-planktonic bacteria (*P. gingivalis*, *F. nucleatum*, and *S. gordonii*) treated with different GelMA hydrogels for 24 h. Scale bars: 10 μm (d). ***$p < 0.001$. (For interpretation of the references to color in this figure legend, the reader is referred to the Web version of this article.)

Oxygen-rich microenvironments may promote ROS generation within anaerobes, which serves as a powerful antimicrobial agent by directly damaging DNA, lipids, and proteins [69,70]. This assumption was validated by staining multi-planktonic bacteria treated with various GelMA hydrogels for 24 h with DCFH-DA. The CAMs@GelMA group displayed intense green fluorescence, while minimal fluorescence was detected in the GelMA and AMs@GelMA groups (Fig. 6d). This was consistent with hypoxyprobe immunofluorescence staining, which showed strong fluorescence signals in the GelMA and AMs@GelMA groups but weak fluorescence in the CAMs@GelMA group (Fig. S4). In summary, these findings suggest that the oxygen released from photosynthetic hydrogels can disrupt the hypoxic environment favorable for anaerobic bacteria and enhance ROS production, thereby exerting selective antibacterial effects on anaerobic oral pathogens.

3.7. Antibiofilm effects of photosynthetic hydrogel on multispecies biofilms

S. gordonii, *P. gingivalis*, and *F. nucleatum* exhibit synergistic interactions that facilitate the formation of well-organized biofilms [71]. 3D live/dead staining images depicted multispecies biofilms with dense green fluorescence in the GelMA and AMs@GelMA groups. In contrast, the distribution of biofilms in the CAMs@GelMA group appeared more dispersed, with a notably reduced proportion of living bacteria (Fig. 7a–c). The average thickness of biofilms further demonstrated a decrease from 11.9 μm (GelMA group) to 5.9 μm (CAMs@GelMA group) for biofilm formation inhibition and a reduction from 19.6 μm (GelMA group) to 6.2 μm (CAMs@GelMA group) for mature biofilm eradication (Fig. 7b–d). Correspondingly, SEM images displayed that compact, polymicrobial biofilms were established in the GelMA and AMs@GelMA groups, whereas bacteria were loosely dispersed after treatment with the CAMs@GelMA hydrogel (Fig. e, f). These findings presented here

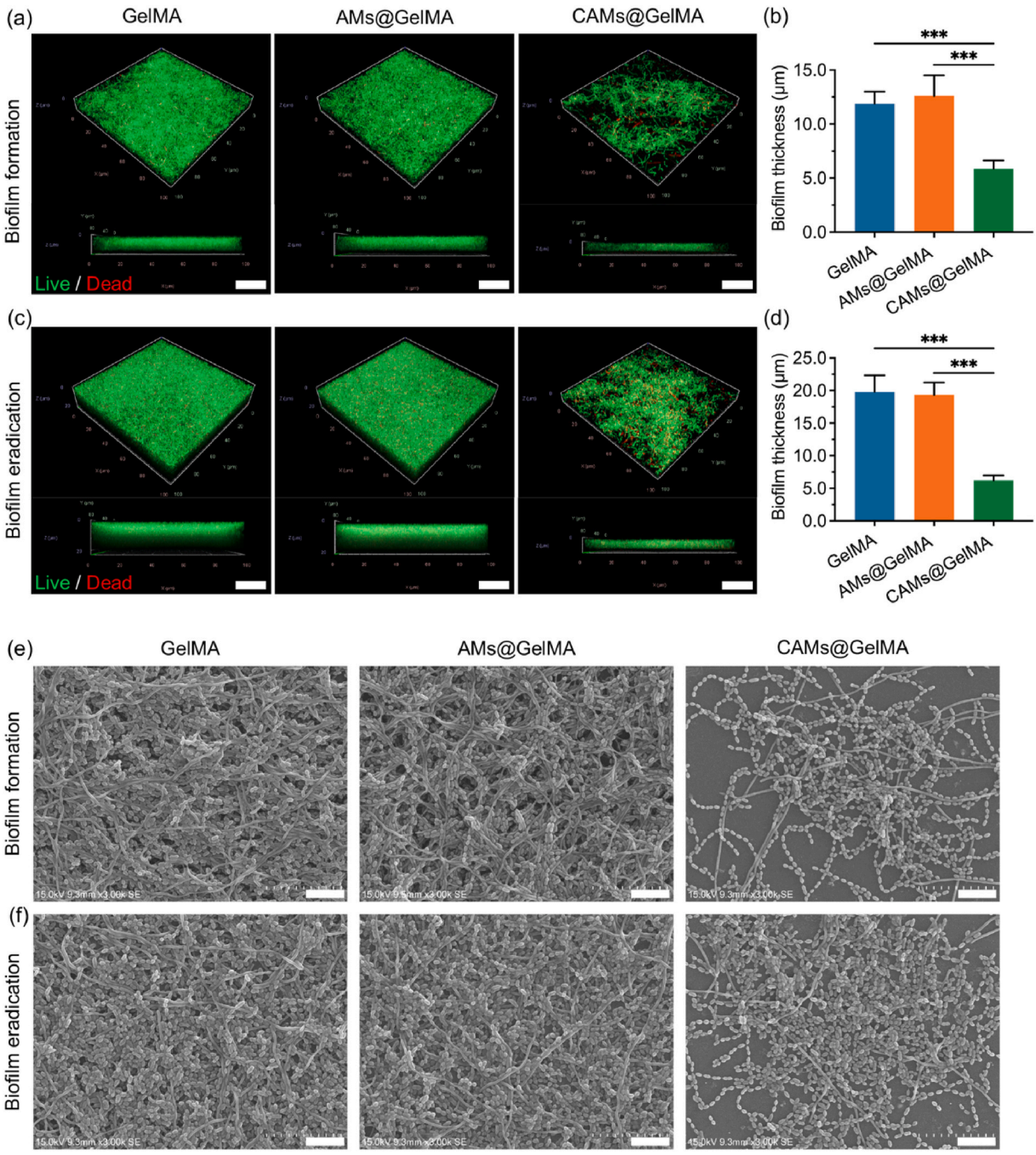

Fig. 7. Antibiofilm effects of photosynthetic hydrogel on multispecies biofilms. (a, c) Representative 3D fluorescent images of live/dead staining for multispecies biofilms treated with different GelMA hydrogels. (b, d) Average thickness of biofilms. (e, f) Representative SEM images of multispecies biofilms treated with different GelMA hydrogels. Scale bars: 5 μm (e, f), 20 μm (a, c). ***$p < 0.001$.

demonstrate the inhibitory and destructive effects of photosynthetic hydrogels on multispecies biofilms, which align with our recent publication on the use of calcium peroxide-loaded GelMA hydrogels for preventing biofilm formation and eliminating subgingival multispecies biofilms through oxygen generation [39].

In this study, *C. reinhardtii* was selected due to its exceptional biocompatibility and well-established characterization. Classified as "Generally Regarded As Safe" (GRAS) by the U.S. Food and Drug Administration (FDA), it does not harbor pathogenic viruses or toxic molecules [40]. Animal studies have demonstrated that *C. reinhardtii* does not elicit significant local or systemic immune responses [32,72]. Furthermore, it is the only photosynthetic microorganism with established clinical safety in human patients after implantation [26]. However, additional research on the biosafety and immunocompatibility of this photosynthetic biomaterial is essential for future clinical translations. After achieving functional vascularization, the issue of microalgae elimination from the host should be addressed. Previous studies have indicated that microalgae survival is limited to less than 14 days *in vivo*, and macrophages can degrade them through phagocytosis [32,73]. Future strategies for microalgae clearance may include using microalgae modified with suicide genes and light deprivation protocols post-treatment. Oxygen concentrations vary among tissues depending on their functions, metabolic requirements, and vasculature. Compared to other oxygen-supplying systems, photosynthetic biomaterials can

offer a sustained and controlled oxygen supply by adjusting microalgae density and illumination parameters (e.g., intensity and wavelengths). They also establish a symbiotic recycling system in which microalgae consume metabolic waste, like CO_2, from mammalian cells while producing oxygen and beneficial organic carbon metabolites. Importantly, this process does not generate cytotoxic byproducts, such as H_2O_2 and ROS [74,75]. Moreover, genetically engineered microalgae capable of generating pro-regenerative bioactive molecules along with oxygen could be utilized to facilitate tissue regeneration [76]. However, providing a light source for internal tissue regeneration *in vivo* remains a significant challenge, as photosynthesis requires direct light exposure, which may be hindered by surrounding tissues. One potential solution is using near-infrared light (NIR) at 980 nm, which possesses remarkable tissue penetration capacity. By irradiating upconversion nanoparticles, NIR can be converted into visible light suitable for photosynthesis [77,78]. Additionally, a 650 nm laser, as an alternative to white light, could be utilized by microalgae for photosynthesis [79], and has been proven to transmit through teeth [80]. These illumination strategies offer promising prospects for applying photosynthetic hydrogels in oral and maxillofacial tissue regeneration. Further investigation into these approaches and exploration of additional potential methods to facilitate *in vivo* photosynthesis will undoubtedly contribute valuable insights to the development of photosynthetic therapy within the realm of tissue regeneration.

4. Conclusion

In summary, *C. reinhardtii* demonstrated excellent photosynthetic activity and biocompatibility. CAMs@GelMA hydrogel could generate a sustainable and sufficient oxygen supply, supporting DPSC metabolic activity and viability. Furthermore, the CAMs@GelMA hydrogel exhibited potent antibacterial and antibiofilm activities against oral anaerobes. The microalgae-based photosynthetic strategy holds great potential to address hypoxia-associated challenges in oral and maxillofacial tissue regeneration. Nevertheless, more studies are required to evaluate the efficacy and feasibility of this photosynthetic biomaterial in relevant animal models and, potentially, in future clinical translation.

CRediT authorship contribution statement

Jun Kang: Writing – original draft, Methodology, Investigation, Data curation, Conceptualization. **Ye Liang:** Validation, Methodology, Investigation. **Junqing Liu:** Methodology, Investigation, Data curation. **Mingxin Hu:** Validation, Investigation. **Shulan Lin:** Formal analysis, Data curation. **Jialin Zhong:** Resources, Methodology. **Chaogang Wang:** Writing – review & editing, Resources. **Qinglu Zeng:** Writing – review & editing, Methodology. **Chengfei Zhang:** Writing – review & editing, Supervision, Project administration, Funding acquisition, Conceptualization.

Declaration of competing interest

The authors declare that they have no known competing financial interests or personal relationships that could have appeared to influence the work reported in this paper.

Data availability

Data will be made available on request.

Acknowledgments

We gratefully acknowledge Dr. José Tomás Egaña, Associate Professor of Institute for Biological and Medical Engineering, Universidad Católica de Chile, for his contribution to the critical review of the manuscript. This work was supported by Seed Funding for Strategic Interdisciplinary Research Scheme from the University Research Committee of the University of Hong Kong, General Research Fund (GRF) grants from the Research Grants Council of Hong Kong (17124821, 17105422) to CF ZHANG.

Appendix B. Supplementary data

Supplementary data to this article can be found online at https://doi.org/10.1016/j.mtbio.2024.101197.

References

[1] W.L. Dissanayaka, L. Zhu, K.M. Hargreaves, L. Jin, C. Zhang, Scaffold-free prevascularized microtissue spheroids for pulp regeneration, J. Dent. Res. 93 (2014) 1296–1303.
[2] Q. Zhang, T. Yang, R. Zhang, X. Liang, G. Wang, Y. Tian, L. Xie, W. Tian, Platelet lysate functionalized gelatin methacrylate microspheres for improving angiogenesis in endodontic regeneration, Acta Biomater. 136 (2021) 441–455.
[3] G. Cheng, S. Guo, M. Li, S. Xiao, B. Jiang, Y. Ding, Hydroxyapatite-coated small intestinal submucosa membranes enhanced periodontal tissue regeneration through immunomodulation and osteogenesis via BMP-2/Smad signaling pathway, Adv. Healthc. Mater. 13 (2023) e2301479.
[4] J. Luo, H. Chen, G. Wang, J. Lyu, Y. Liu, S. Lin, M. Zhou, X. Jiang, CGRP-loaded porous microspheres protect BMSCs for alveolar bone regeneration in the periodontitis microenvironment, Adv. Healthc. Mater. 12 (2023) e2301366.
[5] H. Wang, Y. Xu, P. Wang, J. Ma, P. Wang, X. Han, Y. Fan, D. Bai, Y. Sun, X. Zhang, Cell-mediated injectable blend hydrogel-BCP ceramic scaffold for *in situ* condylar osteochondral repair, Acta Biomater. 123 (2021) 364–378.
[6] K. Nam, C.S. Wang, C.L.M. Maruyama, P. Lei, S.T. Andreadis, O.J. Baker, L1 peptide-conjugated fibrin hydrogels promote salivary gland regeneration, J. Dent. Res. 96 (2017) 798–806.
[7] R. Augustine, M. Gezek, N. Seray Bostanci, A. Nguyen, G. Camci-Unal, Oxygen-generating scaffolds: one step closer to the clinical translation of tissue engineered products, Chem. Eng. J. 455 (2023) 140783.
[8] A. Carreau, B. El Hafny-Rahbi, A. Matejuk, C. Grillon, C. Kieda, Why is the partial oxygen pressure of human tissues a crucial parameter? Small molecules and hypoxia, J. Cell Mol. Med. 15 (2011) 1239–1253.
[9] T. Rademakers, J.M. Horvath, C.A. van Blitterswijk, V.L.S. LaPointe, Oxygen and nutrient delivery in tissue engineering: approaches to graft vascularization, J. Tissue Eng. Regen. Med. 13 (2019) 1815–1829.
[10] Y.J. Blinder, A. Freiman, N. Raindel, D.J. Mooney, S. Levenberg, Vasculogenic dynamics in 3D engineered tissue constructs, Sci. Rep. 5 (2015) 17840.
[11] P.L. Tremblay, V. Hudon, F. Berthod, L. Germain, F.A. Auger, Inosculation of tissue-engineered capillaries with the host's vasculature in a reconstructed skin transplanted on mice, Am. J. Transplant. 5 (2005) 1002–1010.
[12] S.M. Ehsan, S.C. George, Nonsteady state oxygen transport in engineered tissue: implications for design, Tissue Eng. Part A 19 (2013) 1433–1442.
[13] R.H. Eldisoky, S.A. Younes, S.S. Omar, H.S. Gharib, T.A. Tamara, Hyperbaric oxygen therapy efficacy on mandibular defect regeneration in rats with diabetes mellitus: an animal study, BMC Oral Health 23 (2023) 101.
[14] B. Huang, M. Chen, J. Tian, Y. Zhang, Z. Dai, J. Li, W. Zhang, Oxygen-carrying and antibacterial fluorinated nano-hydroxyapatite incorporated hydrogels for enhanced bone regeneration, Adv. Healthc. Mater. 11 (2022) e2102540.
[15] Y. Xiong, Z.Z. Liu, R. Georgieva, K. Smuda, A. Steffen, M. Sendeski, A. Voigt, A. Patzak, H. Bäumler, Nonvasoconstrictive hemoglobin particles as oxygen carriers, ACS Nano 7 (2013) 7454–7461.
[16] T. Zou, S. Jiang, Y. Zhang, J. Liu, B. Yi, Y. Qi, W.L. Dissanayaka, C. Zhang, *In situ* oxygen generation enhances the SCAP survival in hydrogel constructs, J. Dent. Res. 100 (2021) 1127–1135.
[17] B.S. Harrison, D. Eberli, S.J. Lee, A. Atala, J.J. Yoo, Oxygen producing biomaterials for tissue regeneration, Biomaterials 28 (2007) 4628–4634.
[18] Y. Guan, N. Gao, H. Niu, Y. Dang, J. Guan, Oxygen-release microspheres capable of releasing oxygen in response to environmental oxygen level to improve stem cell survival and tissue regeneration in ischemic hindlimbs, J. Contr. Release 331 (2021) 376–389.
[19] C. Plafki, P. Peters, M. Almeling, W. Welslau, R. Busch, Complications and side effects of hyperbaric oxygen therapy, Aviat Space Environ. Med. 71 (2000) 119–124.
[20] N.G.A. Willemen, S. Hassan, M. Gurian, J. Li, I.E. Allijn, S.R. Shin, J. Leijten, Oxygen-releasing biomaterials: current challenges and future applications, Trends Biotechnol. 39 (2021) 1144–1159.
[21] A.A. Venn, J.E. Loram, A.E. Douglas, Photosynthetic symbioses in animals, J. Exp. Bot. 59 (2008) 1069–1080.
[22] J.S. Ortega, R. Corrales-Orovio, P. Ralph, J.T. Egana, C. Gentile, Photosynthetic microorganisms for the oxygenation of advanced 3D bioprinted tissues, Acta Biomater. 165 (2023) 180–196.
[23] Y. Wang, Y. Xue, T. Zhang, Q. Fang, M. Jin, X. Wang, Z. Wang, Y. Hu, W. Zhao, D. Lou, W.Q. Tan, Photosynthetic biomaterials: applications of photosynthesis in algae as oxygenerator in biomedical therapies, Bio-Des, Manuf 4 (2021) 596–611.
[24] E.H. Harris, *Chlamydomonas* as a model organism, Annu. Rev. Plant Biol. 52 (2001) 363–406.

[25] R. Corrales-Orovio, F. Carvajal, C. Holmes, M. Miranda, S. Gonzalez-Itier, C. Cardenas, C. Vera, T.L. Schenck, J.T. Egana, Development of a photosynthetic hydrogel as potential wound dressing for the local delivery of oxygen and bioactive molecules, Acta Biomater. 155 (2023) 154–166.

[26] M.L. Obaid, J.P. Camacho, M. Brenet, R. Corrales-Orovio, F. Carvajal, X. Martorell, C. Werner, V. Simon, J. Varas, W. Calderon, C.D. Guzman, M.R. Bono, S. San Martin, A. Eblen-Zajjur, J.T. Egana, A first in human trial implanting microalgae shows safety of photosynthetic therapy for the effective treatment of full thickness skin wounds, Front. Med. 8 (2021) 772324.

[27] S. Maharjan, J. Alva, C. Cámara, A.G. Rubio, D. Hernández, C. Delavaux, E. Correa, M.D. Romo, D. Bonilla, M.L. Santiago, W. Li, F. Cheng, G. Ying, Y.S. Zhang, Symbiotic photosynthetic oxygenation within 3D-bioprinted vascularized tissues, Matter 4 (2021) 217–240.

[28] A. Lode, F. Krujatz, S. Brüggemeier, M. Quade, K. Schütz, S. Knaack, J. Weber, T. Bley, M. Gelinsky, Green bioprinting: fabrication of photosynthetic algae-laden hydrogel scaffolds for biotechnological and medical applications, Eng. Life Sci. 15 (2015) 177–183.

[29] L.J. Voss, M. Plouviez, N. Whittle, Microalgae-based photosynthetic strategy for oxygenating avascularised mouse brain tissue - an *in vitro* proof of concept study, Brain Res. 1768 (2021) 147585.

[30] C. Holmes, J. Varas, S. San Martin, J.T. Egana, Towards an *in vitro* 3D model for photosynthetic cancer treatment: a study of microalgae and tumor cell interactions, Int. J. Mol. Sci. 23 (2022) 13550.

[31] V. Veloso-Gimenez, R. Escamilla, D. Necunir, R. Corrales-Orovio, S. Riveros, C. Marino, C. Ehrenfeld, C.D. Guzman, M.P. Boric, R. Rebolledo, J.T. Egana, Development of a novel perfusable solution for *ex vivo* preservation: towards photosynthetic oxygenation for organ transplantation, Front. Bioeng. Biotechnol. 9 (2021) 796157.

[32] M.N. Chavez, T.L. Schenck, U. Hopfner, C. Centeno-Cerdas, I. Somlai-Schweiger, C. Schwarz, H.G. Machens, M. Heikenwalder, M.R. Bono, M.L. Allende, J. Nickelsen, J.T. Egana, Towards autotrophic tissue engineering: photosynthetic gene therapy for regeneration, Biomaterials 75 (2016) 25–36.

[33] J.L. Baker, B. Bor, M. Agnello, W. Shi, X. He, Ecology of the oral microbiome: beyond bacteria, Trends Microbiol. 25 (2017) 362–374.

[34] J. Sun, Q. Tang, S. Yu, M. Xie, Y. Xie, G. Chen, L. Chen, Role of the oral microbiota in cancer evolution and progression, Cancer Med. 9 (2020) 6306–6321.

[35] A.B. Berezow, R.P. Darveau, Microbial shift and periodontitis, Periodontol 55 (2011) 36–47, 2000.

[36] M. Sakko, L. Tjäderhane, R. Rautemaa-Richardson, Microbiology of root canal infections, Prim. Dent. J. 5 (2016) 84–89.

[37] S. Gupta, P. Mujawdiya, G. Maheshwari, S. Sagar, Dynamic role of oxygen in wound healing: a microbial, immunological, and biochemical perspective, Arch. Razi Inst. 77 (2022) 513–523.

[38] P.I. Diaz, A.H. Rogers, The effect of oxygen on the growth and physiology of *Porphyromonas gingivalis*, Oral Microbiol. Immunol. 19 (2004) 88–94.

[39] T. Zou, Y. Liang, J. Kang, J. Liu, W. Kang, S. Jiang, C. Zhang, Oxygen enrichment mediated by calcium peroxide loaded gelatin methacrylate hydrogel eradicates periodontal biofilms, Int. J. Biol. Macromol. 265 (2024) 130868.

[40] E.H. Harris, D.B. Stern, G.B. Witman, *Chlamydomonas* in the laboratory, in: E. H. Harris, D.B. Stern, G.B. Witman (Eds.), The *Chlamydomonas* Sourcebook, second ed., Academic Press, San Diego, 2009, pp. 241–302.

[41] T.T. Nazos, D.F. Ghanotakis, Biodegradation of phenol by alginate immobilized *Chlamydomonas reinhardtii* cells, Arch. Microbiol. 203 (2021) 5805–5816.

[42] S.M. Kang, G.W. Lee, Y.S. Huh, Centrifugal force-driven modular micronozzle system: generation of engineered alginate microspheres, Sci. Rep. 9 (2019) 12776.

[43] J.W. Nichol, S.T. Koshy, H. Bae, C.M. Hwang, S. Yamanlar, A. Khademhosseini, Cell-laden microengineered gelatin methacrylate hydrogels, Biomaterials 31 (2010) 5536–5544.

[44] M. Sato, Y. Murata, M. Mizusawa, H. Iwahashi, S.I. Oka, A simple and rapid dual-fluorescence viability assay for microalgae, Microbiol. Cult. Coll. 20 (2004) 53–59.

[45] Q. Chen, M. Qi, F. Shi, C. Liu, Y. Shi, Y. Sun, X. Bai, L. Wang, X. Sun, B. Dong, C. Li, Novel twin-crystal nanosheets with MnO_2 modification to combat bacterial biofilm against periodontal infections via multipattern strategies, Adv. Healthc. Mater. 12 (2023) e2300313.

[46] S. Kalimuthu, B.P.K. Cheung, J.Y.Y. Yau, K. Shanmugam, A.P. Solomon, P. Neelakantan, A novel small molecule, 1,3-di-m-tolyl-urea, inhibits and disrupts multispecies oral biofilms, Microorganisms 8 (2020) 1261.

[47] E. Heber-Katz, Oxygen, metabolism, and regeneration: lessons from mice, Trends Mol. Med. 23 (2017) 1024–1036.

[48] X. Shi, J. Mao, Y. Liu, Pulp stem cells derived from human permanent and deciduous teeth: biological characteristics and therapeutic applications, Stem Cells Transl. Med. 9 (2020) 445–464.

[49] J. Fan, H. Cai, S. Yang, L. Yan, W. Tan, Comparison between the effects of normoxia and hypoxia on antioxidant enzymes and glutathione redox state in *ex vivo* culture of CD34(+) cells, Comp. Biochem. Physiol. B Biochem. Mol. Biol. 151 (2008) 153–158.

[50] M.N. Chavez, B. Fuchs, N. Moellhoff, D. Hofmann, L. Zhang, T.T. Selao, R. E. Giunta, J.T. Egana, J. Nickelsen, T.L. Schenck, Use of photosynthetic transgenic cyanobacteria to promote lymphangiogenesis in scaffolds for dermal regeneration, Acta Biomater. 126 (2021) 132–143.

[51] A. Boveris, L.E. Costa, E. Cadenas, J.J. Poderoso, Regulation of mitochondrial respiration by adenosine diphosphate, oxygen, and nitric oxide, Methods Enzymol. 301 (1999) 188–198.

[52] D. Wangpraseurt, S. You, F. Azam, G. Jacucci, O. Gaidarenko, M. Hildebrand, M. Kühl, A.G. Smith, M.P. Davey, A. Smith, Bionic 3D printed corals, Nat. Commun. 11 (2020) 1748.

[53] H. Chen, Y. Cheng, J. Tian, P. Yang, X. Zhang, Y. Chen, Y. Hu, J. Wu, Dissolved oxygen from microalgae-gel patch promotes chronic wound healing in diabetes, Sci. Adv. 6 (2020) eaba4311.

[54] T.J. Zhou, L. Xing, Y.T. Fan, P.F. Cui, H.L. Jiang, Light triggered oxygen-affording engines for repeated hypoxia-resistant photodynamic therapy, J. Contr. Release 307 (2019) 44–54.

[55] Y. Kang, L. Xu, J. Dong, X. Yuan, J. Ye, Y. Fan, B. Liu, J. Xie, X. Ji, Programmed microalgae-gel promotes chronic wound healing in diabetes, Nat. Commun. 15 (2024) 1042.

[56] Y. Fu, X. Xie, Y. Wang, J. Liu, Z. Zheng, D.L. Kaplan, X. Wang, Sustained photosynthesis and oxygen generation of microalgae-embedded silk fibroin gydrogels, ACS Biomater. Sci. Eng. 7 (2021) 2734–2744.

[57] L. Vazquez-Ayala, C. Del Angel-Olarte, D.M. Escobar-Garcia, S. Rosales-Mendoza, I. Solis-Andrade, A. Pozos-Guillen, G. Palestino, Chitosan sponges loaded with metformin and microalgae as dressing for wound healing: a study in diabetic bio-models, Int. J. Biol. Macromol. 254 (2024) 127691.

[58] I. Moreno-Garrido, Microalgae immobilization: current techniques and uses, Bioresour. Technol. 99 (2008) 3949–3964.

[59] K. Yue, G. Trujillo-de Santiago, M.M. Alvarez, A. Tamayol, N. Annabi, A. Khademhosseini, Synthesis, properties, and biomedical applications of gelatin methacryloyl (GelMA) hydrogels, Biomaterials 73 (2015) 254–271.

[60] C. Schmitz, I. Pepelanova, C. Ude, A. Lavrentieva, Studies on oxygen availability and the creation of natural and artificial oxygen gradients in gelatin-methacryloyl hydrogel 3D cell culture, J. Tissue Eng. Regen. Med. 16 (2022) 977–986.

[61] K. Kellner, G. Liebsch, I. Klimant, O.S. Wolfbeis, T. Blunk, M.B. Schulz, A. Gopferich, Determination of oxygen gradients in engineered tissue using a fluorescent sensor, Biotechnol. Bioeng. 80 (2002) 73–83.

[62] J.R.K. Samal, V.K. Rangasami, S. Samanta, O.P. Varghese, O.P. Oommen, Discrepancies on the role of oxygen gradient and culture condition on mesenchymal stem cell fate, Adv. Healthc. Mater. 10 (2021) e2002058.

[63] B.J. Paster, I. Olsen, J.A. Aas, F.E. Dewhirst, The breadth of bacterial diversity in the human periodontal pocket and other oral sites, Periodontol 42 (2006) 80–87, 2000.

[64] N. Pan, J.A. Imlay, How does oxygen inhibit central metabolism in the obligate anaerobe *Bacteroides thetaiotaomicron*, Mol. Microbiol. 39 (2001) 1562–1571.

[65] S. Marchant, S.R. Brailsford, A.C. Twomey, G.J. Roberts, D. Beighton, The predominant microflora of nursing caries lesions, Caries Res. 35 (2001) 397–406.

[66] A. Sakanaka, H. Takeuchi, M. Kuboniwa, A. Amano, Dual lifestyle of *Porphyromonas gingivalis* in biofilm and gingival cells, Microb, Pathog 94 (2016) 42–47.

[67] J. Mysak, S. Podzimek, P. Sommerova, Y. Lyuya-Mi, J. Bartova, T. Janatova, J. Prochazkova, J. Duskova, *Porphyromonas gingivalis*: major periodontopathic pathogen overview, J. Immunol. Res. 2014 (2014) 476068.

[68] S. Ndongo, S. Khelaifia, J.C. Lagier, D. Raoult, From anaerobes to aerointolerant prokaryotes, Hum. Microbiome J. 15 (2020) 100068.

[69] B. Ezraty, A. Gennaris, F. Barras, J.F. Collet, Oxidative stress, protein damage and repair in bacteria, Nat. Rev. Microbiol. 15 (2017) 385–396.

[70] H. Li, X. Zhou, Y. Huang, B. Liao, L. Cheng, B. Ren, Reactive oxygen species in pathogen clearance: the killing mechanisms, the adaption response, and the side effects, Front. Microbiol. 11 (2020) 622534.

[71] P.E. Kolenbrander, R.N. Andersen, D.S. Blehert, P.G. Egland, J.S. Foster, R. J. Palmer Jr., Communication among oral bacteria, Microbiol. Mol. Biol. Rev. 66 (2002) 486–505.

[72] T.L. Schenck, U. Hopfner, M.N. Chavez, H.G. Machens, I. Somlai-Schweiger, R. E. Giunta, A.V. Bohne, J. Nickelsen, M.L. Allende, J.T. Egana, Photosynthetic biomaterials: a pathway towards autotrophic tissue engineering, Acta Biomater. 15 (2015) 39–47.

[73] F. Zhang, J. Zhuang, Z. Li, H. Gong, B.E. de Ávila, Y. Duan, Q. Zhang, J. Zhou, L. Yin, E. Karshalev, W. Gao, V. Nizet, R.H. Fang, L. Zhang, J. Wang, Nanoparticle-modified microrobots for *in vivo* antibiotic delivery to treat acute bacterial pneumonia, Nat. Mater. 21 (2022) 1324–1332.

[74] Z. Wang, T. Chen, X. Li, B. Guo, P. Liu, Z. Zhu, R.X. Xu, Oxygen-releasing biomaterials for regenerative medicine, J. Mater. Chem. B 11 (2023) 7300–7320.

[75] S. Bayraktar, C. Ustun, N.S. Kehr, Oxygen delivery biomaterials in wound healing applications, Macromol. Biosci. 24 (2024) e2300363.

[76] S. Rosales-Mendoza, L.M. Paz-Maldonado, R.E. Soria-Guerra, *Chlamydomonas reinhardtii* as a viable platform for the production of recombinant proteins: current status and perspectives, Plant Cell Rep. 31 (2012) 479–494.

[77] Y. Zhang, H. Liu, X. Dai, H. Li, X. Zhou, S. Chen, J. Zhang, X.J. Liang, Z. Li, Cyanobacteria-based near-infrared light-excited self-supplying oxygen system for enhanced photodynamic therapy of hypoxic tumors, Nano Res. 14 (2020) 667–673.

[78] J. Wang, Q. Su, Q. Lv, B. Cai, X. Xiaohalati, G. Wang, Z. Wang, L. Wang, Oxygen-generating cyanobacteria powered by upconversion-nanoparticles-converted near-infrared light for ischemic stroke treatment, Nano Lett. 21 (2021) 4654–4665.

[79] W. Li, D. Zhong, S. Hua, Z. Du, M. Zhou, Biomineralized biohybrid algae for tumor hypoxia modulation and cascade radio-photodynamic therapy, ACS Appl. Mater. Interfaces 12 (2020) 44541–44553.

[80] T.M. Odor, N.P. Chandler, T.F. Watson, T.R. Ford, F. McDonald, Laser light transmission in teeth: a study of the patterns in different species, Int. Endod. J. 32 (1999) 296–302.